J Eng Math (2008) 60:69–87
DOI 10.1007/s10665-006-9133-3

The mathematical modelling of rotating capillary tubes for holey-fibre manufacture

C. J. Voyce · A. D. Fitt · T. M. Monro

Received: 14 June 2005 / Accepted: 19 December 2006 / Published online: 21 April 2007

Abstract Understanding and controlling the manufacturing process of producing ("drawing") microstructured optical fibres ("holey fibres") is of paramount importance in obtaining optimal control of the final fibre geometry and identifying industrially useful production regimes. The high cost of the manufacturing process and the challenge of ensuring reproducible final fibre geometries renders theoretical approaches invaluable. In this study the fluid dynamics of capillary drawing is examined using an extensional-flow asymptotic approach based on the small aspect ratio of the capillary. The key focus of the study is the additional effects that may be introduced by adding fibre rotation to the manufacturing process. Predictions are made concerning the effects of rotation, and a variety of asymptotic limits are examined in order to gain an understanding of the physics involved. Drawing regimes that are useful from a practical point of view are identified and the role of fibre rotation, both as a control measure (that may be used to influence the final geometry of a capillary) and as a means of reducing unwanted effects (such as fibre birefringence and polarisation model dispersion), is discussed.

Keywords Asymptotic analysis · Fibre rotation · Holey fibres · PMD

1 Introduction

Microstructured optical fibres ("holey fibres") have lately invoked great interest. Such fibres typically consist of a lattice of air-filled holes, which may take many different forms, arranged around a solid core, such as the one pictured in Fig. 1. The presence of air holes lowers the effective refractive index of the cladding, and the effective refractive-index difference between the solid core and the air/glass lattice allows the fibre to guide light [1–3]. Holey fibres are manufactured by heating a macroscopic preform and drawing it down (decreasing its diameter) into fibre form. Because of the complex hole-structure involved, experimental experience has invariably confirmed that the process of holey-fibre fabrication depends on the draw parameters in an extremely sensitive fashion. From a manufacturing point of view, it is cost-effective to be able to produce a range of different fibres from a single

C. J. Voyce · A. D. Fitt (✉)
School of Mathematics, University of Southampton, Southampton SO17 1BJ, UK
e-mail: adf@maths.soton.ac.uk

T. M. Monro
School of Chemistry & Physics, University of Adelaide, Adelaide, SA 5005, Australia

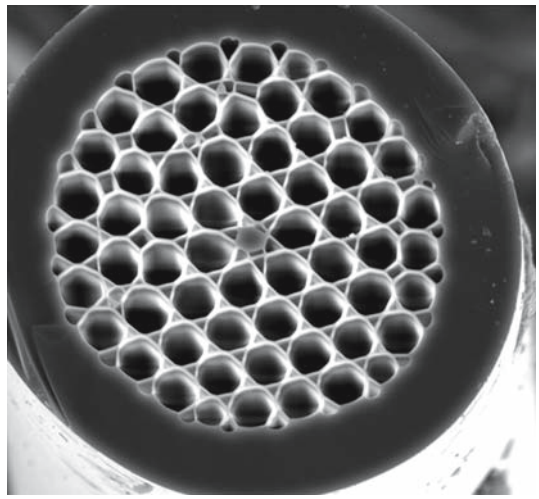

Fig. 1 Magnified cross-section photograph of one of the many different types of typical holey fibre

preform. A theoretical understanding of the relative effects of changes in one or more of the draw parameters is thus required so that the fibre geometry (and in particular the "draw-down ratio", which characterises the fibre-geometry change during drawing) may be tailored by varying the draw parameters, thus influencing the optical properties of the fibre.

Many holey fibres produced to date display Polarisation Mode Dispersion (PMD) and fibre birefringence effects (which may be desirable but are more often unwanted). It will be explained below how rotating the fibre as it enters the furnace may eliminate such effects; for this reason, fibre rotation is the main focus of the current study.

In the manufacture of conventional (solid) optical fibres, a solid preform (whose diameter is typically a few centimetres) is constructed and drawn down to the desired final dimensions (typically about 125 μm). Though the main physical processes of holey-fibre drawing are superficially identical to the solid case, the complex interplay between surface tension and viscosity in the more complicated air/glass preform structure greatly increases the sensitivity of the whole manufacturing process. All practically useful holey fibres contain a large number of holes, and the drawing process is therefore completed in two stages. In the first stage, where the final preform is created, capillary tubes are stacked inside a larger capillary. This initial tube is then drawn down to produce a "cane". After the "caning" stage of production these sections are fitted inside a large capillary. The new preform is then drawn down to the final required dimensions.

1.1 Fibre rotation

Fibre birefringence provides a reason for spinning during the fibre-manufacture process. Its effects can be significant for three main reasons [4]. First, many holey fibres have wavelength-scale structures. Second, a significant contrast may exist between the refractive index of the core and the effective refractive index of the cladding. Finally, the intended or accidental geometrical asymmetries that may be introduced into the manufacturing process may include the "locking-in" of an asymmetric stress distribution within the fibre [3]. When such asymmetries are present in holey fibres, exacerbated by the high refractive-index contrast, the two polarizations of light travel at different speeds. This results in fibre birefringence with a characteristic beat length, caused by the two components of light interfering as they travel at different speeds. Quite apart from birefringence issues, conventional (solid) fibres are routinely rotated to introduce a twist into the final fibre, since this reduces PMD [5–7]. Recently, large mode-area fibres with a high density of small, dispersed holes have been spun at rates sufficient to dramatically reduce PMD [8]. Birefringence is not always unwanted: in sensor applications where maintaining a polarization is desirable to improve isolation between the modes by maximizing the mode splitting, fibre birefringence is desirable. In data transmission and other applications fibre birefringence is unwanted and can be reduced by averaging out the effects

of asymmetries along the fibre by introducing a twist [5]. The periodicity of the twist depends on the wavelength of light involved and the details of the fibre profile.

In practice, fibre rotation may be achieved by rotating the glass preform either as it enters or leaves the furnace. The former is the preferred option, and is usually achieved by attaching an electric drill to the top of the fibre preform [5] and passing the drawn fibre onto a rotating drum. The twist is therefore taken up whilst the fibre is still strictly in the fluid phase and not close to the glass transition temperature (see [5]). The rapid fibre solidification at the furnace exit means that the fibre rotation is essentially fixed at zero at the end of the draw. This leaves the fibre with an overall twist along its length, as required (see, for example, [5], [6] and [9]).

Imparting spin to the fibre as it leaves the furnace appears to be less advantageous as the resulting fibre is circularly birefringent (see, for example, [5]). Rotation of the rapidly cooling fibre as it leaves the drawing furnace allows locked-in stresses to develop. These stresses give rise to further unwanted circular birefringence.

Though ultimately our aim is to model the drawing of holey fibres, in this study we consider the case of a single axisymmetric capillary tube (or a solid fibre) in the hope that the ideas and techniques developed may then be directly extrapolated to more complex holey-fibre structures. Though the rotation of both solid fibres and capillary tubes is clearly of interest for its own sake, we make the implicit assumption that conclusions for a single capillary may further be related to the drawing process for a general holey fibre. Although the general case (where fibres may contain complicated arrays of holes with non-axisymmetric distributions) is too complicated to treat using the model developed below, the "type one" and "type two" analogies introduced in [10] can allow us to infer results that have significance for general microstructured optical fibres. For "type one" fibres (large mode-area holey fibres with an approximately uniform distribution of diffuse holes) it seems reasonable to assume that the geometrical consequences of rotation are closely related to results for a solid fibre. In contrast, for "type two" fibres (fibres with a large density of holes in a small, central region surrounded by a thick jacket-tube) the results for spun capillary tubes are clearly relevant.

Though rotation is routinely used in the manufacture of conventional optical fibres with a solid core and cladding region, the rotation of holey fibres does not seem previously to have been addressed theoretically. The presence of air holes poses questions as to how such fibres will evolve when rotated, further motivating this study.

Extensional-flow modelling for fibre drawing was considered for solid fibres in [11] and a number of other sources. The study of [12] proposed related equations to determine the behaviour of a drawn capillary tube. Here we extend this work still further to allow for fibre rotation. Though rotation of a solid fibre was considered briefly in [11], to the authors' knowledge the current study is the first theoretical attempt to fully characterise the effects of rotation on a capillary tube. Though the rotation of capillaries was discussed briefly in [10], discussion of the detailed asymptotic limits that were relevant to fibre manufacture was necessarily limited.

In contrast to [10], the current analysis will include the effects not only of fibre rotation, but also of surface tension, gravity, internal hole pressurisation (which has previously been used as a control parameter) and fibre inertia. The equations will be solved numerically for general cases. In addition, we will analyse a number of relevant asymptotic limits of the governing equations that have not previously been considered to give physical insight into practically relevant cases, allowing us to determine (for example) whether or not fibre rotation may be used as a control mechanism for preventing surface-tension-driven hole-closure in a drawn capillary. We shall also show that the act of imparting a spin to a capillary as it passes through the furnace affects the final fibre geometry. We not only predict the effects of fibre rotation, but also determine the distance between successive twists, i.e., the twist periodicity ("pitch") in a final drawn fibre.

2 Governing equations for capillary drawing with rotation

To derive governing equations, we assume that the flow is axisymmetric and that the glass may have a temperature-dependent viscosity. In line with many previous studies (see, for example, the discussion in [13]) we also assume that molten glass behaves as a Newtonian fluid. Though it is well-known that as glass begins to solidify it

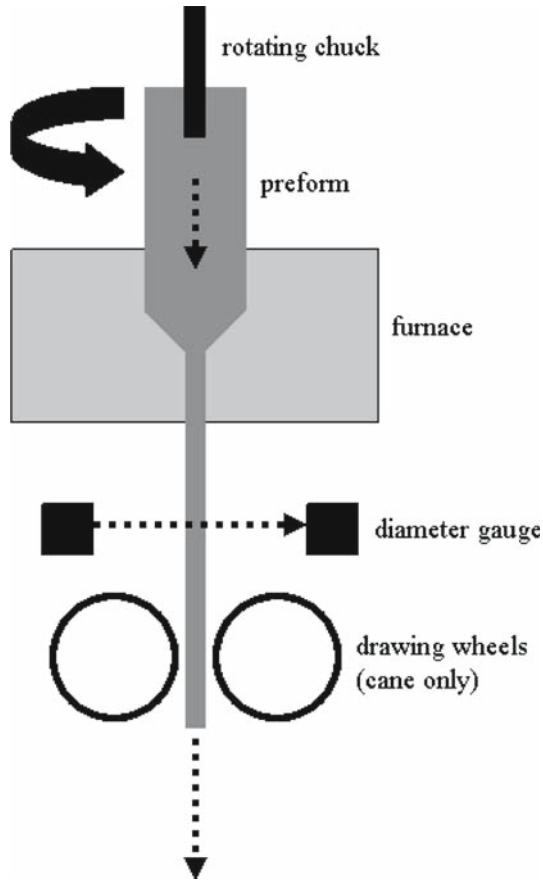

Fig. 2 Typical experimental set-up for fibre drawing with rotation

may exhibit elastic properties, at the temperatures considered in this study most previous authors have ignored the non-Newtonian flow properties of glass.

A typical experimental set-up is shown in Fig. 2. Note that we will always assume that the temperature is user-defined. The Navier–Stokes equations are then (see, for example, [14])

$$\rho(w_t + uw_r + ww_z) = -p_z + \frac{1}{r}(\mu r w_r)_r + \frac{1}{r}(\mu r u_z)_r + 2(\mu w_z)_z + \rho g, \tag{1}$$

$$\rho\left(u_t + uu_r + wu_z - \frac{v^2}{r}\right) = -p_r + \mu\left(\frac{1}{r}(ru)_r\right)_r + (\mu u_z)_z + \mu_z w_r, \tag{2}$$

$$\rho\left(v_t + wv_z + uv_r + \frac{uv}{r}\right) = \mu\left(\frac{1}{r}(rv)_r\right)_r + (\mu v_z)_z, \tag{3}$$

$$\frac{1}{r}(ru)_r + w_z = 0. \tag{4}$$

Here p denotes pressure, g is the acceleration due to gravity, and ρ, μ and γ are the density, dynamic viscosity and surface tension, respectively. Time is denoted by t, and z and r denote distance, respectively, along the capillary axis and perpendicular to it. All t, z and r subscripts denote differentiation, and the fluid velocity is denoted by $\boldsymbol{q} = w\boldsymbol{e}_z + u\boldsymbol{e}_r + v\boldsymbol{e}_\theta$ where $\boldsymbol{e}_z$, $\boldsymbol{e}_r$ and $\boldsymbol{e}_\theta$ are unit vectors in the z, r and θ directions, respectively. Though axisymmetry demands that all quantities are independent of the azimuthal angle θ, in general we consider non-zero v.

Figure 3 shows a schematic diagram of a capillary geometry; B is the angular frequency of the evolving preform, to be defined below. The inner and the outer radii of the capillary are denoted, respectively, by $r = h_i(z, t)$

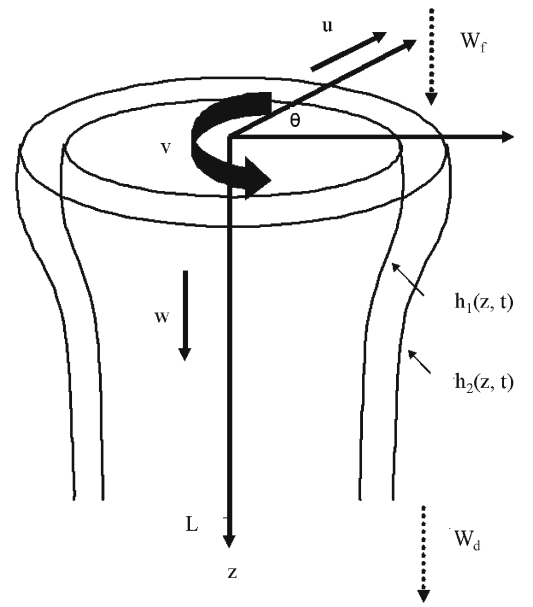

Fig. 3 Schematic diagram of capillary geometry

($i = 1, 2$). The governing equations thus apply in the region $z \in [0, L]$, $r \in [h_1, h_2]$, and for $t \geq 0$, and must be solved subject to suitable boundary and initial conditions (discussed below). The fibre feed and draw speeds are denoted by W_f and W_d, respectively, the ambient pressure in the air surrounding the fibre is denoted by p_a and the pressure of the air in the hole $r < h_1(z, t)$ by p_H.

We non-dimensionalise (1)–(4) by setting $z = L\bar{z}$, $r = h\bar{r}$, $t = (L/W)\bar{t}$, $h_1 = h\bar{h}_1$, $h_2 = h\bar{h}_2$, $\mu = \mu_0\bar{\mu}$, $p = (\mu_0 W/L)\bar{p}$, $w = W\bar{w}$, $u = (hW/L)\bar{u}$, $v = \Omega L\bar{v}$ and $\theta = \bar{\theta}$. Here an overbar denotes a non-dimensional quantity and L denotes a typical hot-zone length in the fibre-drawing furnace. h denotes a typical drawn capillary size, W denotes a typical draw speed and μ_0 denotes a typical glass viscosity. The constant Ω is a measure of the angular frequency of the evolving preform. The equations become

$$\epsilon^2 \mathrm{Re}\,(\bar{w}_{\bar{t}} + \bar{u}\bar{w}_{\bar{r}} + \bar{w}\bar{w}_{\bar{z}}) = -\epsilon^2 \bar{p}_{\bar{z}} + \frac{1}{\bar{r}}(\bar{\mu}\bar{r}\bar{w}_{\bar{r}})_{\bar{r}} + \epsilon^2(2\bar{\mu}\bar{w}_{\bar{z}})_{\bar{z}} + \frac{\epsilon^2}{\bar{r}}(\bar{\mu}\bar{r}\bar{u}_{\bar{z}})_{\bar{r}} + \frac{\epsilon^2 \mathrm{Re}}{\mathrm{Fr}}, \tag{5}$$

$$\epsilon^2 \mathrm{Re}\left(\bar{u}_{\bar{t}} + \bar{u}\bar{u}_{\bar{r}} + \bar{w}\bar{u}_{\bar{z}} - \frac{S^2\bar{v}^2}{\epsilon^2\bar{r}}\right) = -\bar{p}_{\bar{r}} + \bar{\mu}\left(\frac{1}{\bar{r}}(\bar{r}\bar{u})_{\bar{r}}\right)_{\bar{r}} + \epsilon^2(\bar{\mu}\bar{u}_{\bar{z}})_{\bar{z}} + \bar{\mu}_{\bar{z}}\bar{w}_{\bar{r}}, \tag{6}$$

$$\mathrm{Re}\left(\bar{v}_{\bar{t}} + \bar{w}\bar{v}_{\bar{z}} + \bar{u}\bar{u}_{\bar{r}} + \frac{\bar{u}\bar{v}}{\bar{r}}\right) = \frac{\bar{\mu}}{\epsilon^2}\left(\frac{1}{\bar{r}}(\bar{r}\bar{v})_{\bar{r}}\right)_{\bar{r}} + (\bar{\mu}\bar{v}_{\bar{z}})_{\bar{z}}, \tag{7}$$

$$\frac{1}{\bar{r}}(\bar{r}\bar{u})_{\bar{r}} + \bar{w}_{\bar{z}} = 0, \tag{8}$$

where the key non-dimensional parameters in the problem are given by

$$\epsilon = \frac{h}{L}, \quad \mathrm{Re} = \frac{LW\rho}{\mu_0}, \quad \mathrm{Fr} = \frac{W^2}{gL}, \quad S = \frac{\Omega L}{W}.$$

The natural small parameter in the problem is the aspect ratio $\epsilon = h/L$; in all cases of interest $\epsilon \ll 1$. It is now appropriate to seek expansions of the form

$$\bar{w} = \bar{w}_0(\bar{z}, \bar{t}) + \epsilon^2\bar{w}_1(\bar{z}, \bar{r}, \bar{t}) + \cdots, \quad \bar{u} = \bar{u}_0(\bar{z}, \bar{r}, \bar{t}) + \epsilon^2\bar{u}_1(\bar{z}, \bar{r}, \bar{t}) + \cdots,$$

$$\bar{v} = \bar{v}_0(\bar{z}, \bar{r}, \bar{t}) + \epsilon^2\bar{v}_1(\bar{z}, \bar{r}, \bar{t}) + \cdots, \quad \bar{p} = \frac{\bar{p}_a}{\epsilon^2} + \bar{P}(\bar{z}, \bar{r}, \bar{t}) + \cdots,$$

where $\bar{p}_a$ denotes the non-dimensional ambient pressure, defined by $p_a = (\mu_0 W/L)\bar{p}_a$, and, from the continuity equation,

$$\bar{u}_0 = -\frac{\bar{r}\bar{w}_{0\bar{z}}}{2} + \frac{\bar{A}}{\bar{r}}, \tag{9}$$

where the function $\bar{A}(\bar{z}, \bar{t})$ is to be determined. Since we have assumed that, to leading order, the small aspect ratio of the fibre means that the viscosity is independent of $\bar{r}$, the $\bar{z}$- and $\bar{\theta}$-momentum equations (5) and (7) now become, to leading order,

$$\mathrm{Re}\,(\bar{w}_{0\bar{t}} + \bar{w}_0\bar{w}_{0\bar{z}}) + \bar{P}_{\bar{z}} - \frac{\mathrm{Re}}{\mathrm{Fr}} - 2(\bar{\mu}\bar{w}_{0\bar{z}})_{\bar{z}} + \bar{\mu}\bar{w}_{0\bar{z}\bar{z}} = \frac{\bar{\mu}}{\bar{r}}(\bar{r}\bar{w}_{1\bar{r}})_{\bar{r}}, \tag{10}$$

$$\bar{v}_{0\bar{r}\bar{r}} + \frac{\bar{v}_{0\bar{r}}}{\bar{r}} - \frac{\bar{v}_0}{\bar{r}^2} = 0. \tag{11}$$

Using (9), the $\bar{r}$-momentum equation (6) yields

$$\bar{P}_{\bar{r}} = \frac{\mathrm{Re}S^2\bar{v}_0^2}{\bar{r}}. \tag{12}$$

It is now necessary to specify kinematic and dynamic boundary conditions on the free boundaries $\bar{h}_1$ and $\bar{h}_2$. The kinematic conditions are (for $i = 1, 2$)

$$\bar{u}_0 = \bar{h}_{i\bar{t}} + \bar{w}_0\bar{h}_{i\bar{z}} \quad \text{at} \quad \bar{r} = \bar{h}_i. \tag{13}$$

As noted above, we do not wish to discount the possibility of controlling hole size by internal hole pressurisation as well as rotation. Defining the non-dimensional fibre hole pressure $\bar{p}_H$ by $p_H = (\mu_0 W/L)\bar{p}_H$, we set

$$\bar{p}_H = \frac{\bar{p}_a}{\epsilon^2} + \bar{p}_o, \tag{14}$$

where $\bar{p}_o$ is the non-dimensional hole overpressure. This scaling reflects the fact that, unless the fibre hole pressure is within $O(\epsilon^2)$ of the ambient pressure, the capillary will either collapse or "explode" immediately (see [12,15]). (Note that, here and henceforth, the "Order" notation used above has its usual asymptotic meaning: see, for example, [16, p. 175].) Equation 14 therefore already gives a useful estimate of the size of hole inflation pressure that is required to prevent hole collapse or explosion.

The normal-stress boundary conditions may now be applied. Denoting the non-dimensional stress tensor by $\bar{\mathcal{T}}$ and the dimensionless unit outward-pointing normal to $\bar{r} = \bar{h}_i$ $(i = 1, 2)$ by $\hat{\boldsymbol{n}}_i$, we have

$$-\hat{\boldsymbol{n}}_1^T\bar{\mathcal{T}}\hat{\boldsymbol{n}}_1 + \frac{\bar{\gamma}\mu_0 W}{\bar{h}_1 L} = \frac{\bar{p}_H\mu_0 W}{L} \quad \text{at} \quad \bar{r} = \bar{h}_1, \tag{15}$$

$$-\hat{\boldsymbol{n}}_2^T\bar{\mathcal{T}}\hat{\boldsymbol{n}}_2 - \frac{\bar{\gamma}\mu_0 W}{\bar{h}_2 L} = \frac{\bar{p}_a\mu_0 W}{L\epsilon^2} \quad \text{at} \quad \bar{r} = \bar{h}_2, \tag{16}$$

where the non-dimensional surface tension coefficient $\bar{\gamma}$ has been defined by $\gamma = \mu_0 W\epsilon\bar{\gamma}$, thus immediately giving an estimate of the order of magnitude that the surface tension of the molten glass has to be to influence the final shape of the fibre.

Since the shear stress of the air on the fibre is negligible, we assume that the tangential stress on both of the fibre boundaries is zero. Thus, for $i = 1, 2$

$$\hat{\boldsymbol{t}}_i^T\bar{\mathcal{T}}\hat{\boldsymbol{n}}_i = 0,$$

where $\hat{\boldsymbol{t}}_i$ is either one of the relevant unit tangent vectors.

The normal and tangential stress conditions now give, to leading order,

$$-\frac{\bar{\gamma}}{\bar{h}_1} - \bar{P}_1 + 2\bar{\mu}\bar{u}_{0\bar{r}} + \bar{p}_o = 0 \qquad \text{at} \quad \bar{r} = \bar{h}_1,$$

$$\frac{\bar{\gamma}}{\bar{h}_2} - \bar{P}_2 + 2\bar{\mu}\bar{u}_{0\bar{r}} = 0 \qquad \text{at} \quad \bar{r} = \bar{h}_2,$$

$$2\bar{h}_{i\bar{z}}(\bar{w}_{0\bar{z}} - \bar{u}_{0\bar{r}}) - \bar{u}_{0\bar{z}} = \bar{w}_{1\bar{r}} \quad \text{at } \bar{r} = \bar{h}_i, \quad (i = 1, 2),$$

$$\bar{v}_{1\bar{r}} - \bar{h}_{i\bar{z}}\bar{v}_{0\bar{z}} - \frac{\bar{v}_1}{\bar{r}} = 0 \quad \text{at } \bar{r} = \bar{h}_i \quad (i = 1, 2)$$

where $\bar{P}_i = \bar{P} \mid_{\bar{r}=\bar{h}_i}$.

It is now possible to derive a closed system of leading-order equations for annular fibre drawing with rotation. We first integrate the $\bar{r}$-momentum equation (12), having solved the leading-order $\bar{\theta}$-momentum equation (11) to give, using the boundary conditions,

$$\bar{v}_0 = \bar{B}(\bar{z}, \bar{t})\bar{r}.$$

Thus

$$\bar{P} = \frac{\mathrm{Re}S^2\bar{B}(\bar{z}, \bar{t})^2\bar{r}^2}{2} + \bar{C}(\bar{z}, \bar{t}). \tag{17}$$

The quantity $\bar{B}(\bar{z}, \bar{t})$ may be thought of as the non-dimensional leading-order angular frequency; both $\bar{B}(\bar{z}, \bar{t})$ and $\bar{C}(\bar{z}, \bar{t})$ are as yet unknown constants of integration that will be determined later.

We now multiply the z-momentum equation (10) by $\bar{r}$, integrate from $\bar{r} = \bar{h}_1$ to $\bar{r} = \bar{h}_2$ and use (17) to yield

$$\frac{(\bar{h}_2^2 - \bar{h}_1^2)}{2}\left[\mathrm{Re}(\bar{w}_{0\bar{t}} + \bar{w}_0\bar{w}_{0\bar{z}}) + \bar{C}_{\bar{z}} - \frac{\mathrm{Re}}{\mathrm{Fr}} - 2(\bar{\mu}\bar{w}_{0\bar{z}})_{\bar{z}} + \bar{\mu}\bar{w}_{0\bar{z}\bar{z}}\right]$$
$$= -\frac{\mathrm{Re}S^2(\bar{B}^2)_{\bar{z}}}{8}(\bar{h}_2^4 - \bar{h}_1^4) + (\bar{\mu}\bar{h}_2\bar{w}_{1\bar{r}}) \mid_{\bar{h}_2} - (\bar{\mu}\bar{h}_1\bar{w}_{1\bar{r}}) \mid_{\bar{h}_1}. \tag{18}$$

The kinematic conditions (13) now give, for $i = 1, 2$

$$(\bar{h}_i^2)_{\bar{t}} + (\bar{h}_i^2\bar{w}_0)_{\bar{z}} = 2\bar{A}, \tag{19}$$

and the normal and tangential-stress boundary conditions, when applied at $\bar{r} = \bar{h}_1$ and $\bar{r} = \bar{h}_2$, respectively, give

$$0 = -\frac{\bar{\gamma}}{\bar{h}_1} - \bar{P}_1 + \bar{p}_o + \bar{\mu}\left(-\bar{w}_{0\bar{z}} - \frac{2\bar{A}}{\bar{h}_1^2}\right), \tag{20}$$

$$0 = \frac{\bar{\gamma}}{\bar{h}_2} - \bar{P}_2 + \bar{\mu}\left(-\bar{w}_{0\bar{z}} - \frac{2\bar{A}}{\bar{h}_2^2}\right), \tag{21}$$

$$\bar{w}_{1\bar{r}} \mid_{\bar{r}=\bar{h}_1} = 2\bar{h}_{1\bar{z}}\left(\frac{3\bar{w}_{0\bar{z}}}{2} + \frac{\bar{A}}{\bar{h}_1^2}\right) - \frac{\bar{A}_{\bar{z}}}{\bar{h}_1} + \frac{\bar{h}_1\bar{w}_{0\bar{z}\bar{z}}}{2}, \tag{22}$$

$$\bar{w}_{1\bar{r}} \mid_{\bar{r}=\bar{h}_2} = 2\bar{h}_{2\bar{z}}\left(\frac{3\bar{w}_{0\bar{z}}}{2} + \frac{\bar{A}}{\bar{h}_2^2}\right) - \frac{\bar{A}_{\bar{z}}}{\bar{h}_2} + \frac{\bar{h}_2\bar{w}_{0\bar{z}\bar{z}}}{2}. \tag{23}$$

The $\bar{\theta}$-momentum equation (7) gives

$$\mathrm{Re}\left(\bar{v}_{0\bar{t}} + \bar{u}_0\bar{v}_{0\bar{r}} + \bar{w}_0\bar{v}_{0\bar{z}} + \frac{\bar{u}_0\bar{v}_0}{\bar{r}}\right) = \bar{\mu}\left(\bar{v}_{1\bar{r}\bar{r}} + \frac{\bar{v}_{1\bar{r}}}{\bar{r}} - \frac{\bar{v}_1}{\bar{r}^2}\right) + (\bar{\mu}\bar{v}_{0\bar{z}})_{\bar{z}}. \tag{24}$$

On multiplying through by $\bar{r}^2$ and integrating from $\bar{r} = \bar{h}_1$ to $\bar{r} = \bar{h}_2$, we learn, using the boundary conditions, that

$$\mathrm{Re}\bar{B}_{\bar{t}}(\bar{h}_2^4 - \bar{h}_1^4) - Re\bar{B}\bar{w}_{0\bar{z}}(\bar{h}_2^4 - \bar{h}_1^4) + 4\mathrm{Re}\bar{A}\bar{B}(\bar{h}_2^2 - \bar{h}_1^2) + \mathrm{Re}\bar{B}_{\bar{z}}\bar{w}_0(\bar{h}_2^4 - \bar{h}_1^4) = [\bar{\mu}\bar{B}_{\bar{z}}(\bar{h}_2^4 - \bar{h}_1^4)]_{\bar{z}}. \tag{25}$$

Equations 18–23 and 25, together with the equations for $\bar{P}$ at $\bar{r} = \bar{h}_1$ and $\bar{r} = \bar{h}_2$, respectively, now constitute a system of 10 equations in the 10 unknowns $\bar{h}_1$, $\bar{h}_2$, $\bar{w}_0$, $\bar{P}_1$, $\bar{P}_2$, $\bar{C}$, $\bar{B}$, $\bar{A}$, $\bar{w}_{1r} \mid_{\bar{r}=\bar{h}_1}$ and $\bar{w}_{1r} \mid_{\bar{r}=\bar{h}_2}$. Regarding (20) and (21) as linear equations for $\bar{A}$ and $\bar{C}$, we find that

$$\bar{A} = \frac{\bar{h}_1\bar{h}_2(2p_o\bar{h}_1\bar{h}_2 - 2\bar{\gamma}(\bar{h}_1 + \bar{h}_2) - \mathrm{Re}S^2\bar{B}^2(\bar{h}_2\bar{h}_1^3 - \bar{h}_1\bar{h}_2^3))}{4\bar{\mu}(\bar{h}_2^2 - \bar{h}_1^2)}, \tag{26}$$

$$\bar{C} = \frac{2\gamma(\bar{h}_1 + \bar{h}_2) + 2\bar{\mu}\bar{w}_{0\bar{z}}(\bar{h}_1^2 - \bar{h}_2^2) - 2\bar{p}_o\bar{h}_1^2 + \mathrm{Re}S^2\bar{B}^2(\bar{h}_1^4 - \bar{h}_2^4)}{2(\bar{h}_2^2 - \bar{h}_1^2)}. \tag{27}$$

By use of (22) and (23) in (18), much simplification occurs, and the final non-dimensional equations that govern the drawing of a capillary become

$$\mathrm{Re}(\bar{h}_2^2 - \bar{h}_1^2)(\bar{w}_{0\bar{t}} + \bar{w}_0\bar{w}_{0\bar{z}} - \frac{1}{\mathrm{Fr}}) = \left[3\bar{\mu}(\bar{h}_2^2 - \bar{h}_1^2)\bar{w}_{0\bar{z}} + \bar{\gamma}(\bar{h}_1 + \bar{h}_2) + \frac{1}{4}\mathrm{Re}S^2(\bar{h}_2^4 - \bar{h}_1^4)\bar{B}^2\right]_{\bar{z}}, \tag{28}$$

$$(\bar{h}_1^2)_{\bar{t}} + (\bar{h}_1^2\bar{w}_0)_{\bar{z}} = \frac{\bar{h}_1\bar{h}_2(2\bar{p}_o\bar{h}_1\bar{h}_2 - 2\bar{\gamma}(\bar{h}_1 + \bar{h}_2) + \mathrm{Re}S^2\bar{B}^2\bar{h}_1\bar{h}_2(\bar{h}_2^2 - \bar{h}_1^2))}{2\bar{\mu}(\bar{h}_2^2 - \bar{h}_1^2)}, \tag{29}$$

$$(\bar{h}_2^2)_{\bar{t}} + (\bar{h}_2^2\bar{w}_0)_{\bar{z}} = \frac{\bar{h}_1\bar{h}_2(2\bar{p}_o\bar{h}_1\bar{h}_2 - 2\bar{\gamma}(\bar{h}_1 + \bar{h}_2) + \mathrm{Re}S^2\bar{B}^2\bar{h}_1\bar{h}_2(\bar{h}_2^2 - \bar{h}_1^2))}{2\bar{\mu}(\bar{h}_2^2 - \bar{h}_1^2)}, \tag{30}$$

$$\mathrm{Re}[\bar{h}_2^2(\bar{h}_2^2\bar{B})_{\bar{t}} - \bar{h}_1^2(\bar{h}_1^2\bar{B})_{\bar{t}}] + \mathrm{Re}\bar{w}_0[\bar{h}_2^2(\bar{h}_2^2\bar{B})_{\bar{z}} - \bar{h}_1^2(\bar{h}_1^2\bar{B})_{\bar{z}}] + \frac{\mathrm{Re}\bar{p}_o}{\bar{\mu}}\bar{B}\bar{h}_1^2\bar{h}_2^2$$
$$-\frac{\mathrm{Re}\bar{\gamma}\bar{B}\bar{h}_1\bar{h}_2}{\bar{\mu}}(\bar{h}_1 + \bar{h}_2) + \frac{\mathrm{Re}^2S^2\bar{B}^3\bar{h}_1^2\bar{h}_2^2(\bar{h}_2^2 - \bar{h}_1^2)}{2\bar{\mu}} = \left[\bar{\mu}(\bar{h}_2^4 - \bar{h}_1^4)\bar{B}_{\bar{z}}\right]_{\bar{z}}. \tag{31}$$

To fully close the problem (28)–(31) it is necessary to specify appropriate boundary and initial conditions. It is simplest to assume that h_1, h_2, w_0 and B are all known as functions of z at time $t = 0$; for the majority of this study, however, we will be interested primarily in steady-state fibre manufacture. As far as boundary conditions are concerned, the preform geometry is known and the feed speed is normally prescribed. At the furnace exit different boundary conditions may be appropriate for different regimes of fibre manufacture. For "caning", the capillaries are normally pulled by counter-rotating drawing wheels that travel at a constant speed: see Fig. 2. Some slip may occur between the drawn capillary and the wheels (though most manufacturers deny that this ever happens). Once drawn, the capillaries may later be stacked together to create a preform, and drawn into fibre that is normally pulled onto a rotating drum. It is therefore not quite clear whether the draw speed, the draw force, or a combination of the two is the appropriate condition to prescribe. In the absence of any firm indications to the contrary, we shall proceed under the assumption that the draw speed is prescribed. We shall also normally assume that the fibre is rotated at $\bar{z} = 0$ and held fixed (no rotation) at $\bar{z} = 1$.

Before we further discuss the governing equations, we note that, in dimensional form, with $B = (\Omega/\epsilon)\bar{B}$, Eqs. (28)–(31) become

$$\rho(h_2^2 - h_1^2)(w_{0t} + w_0w_{0z} - g) = \left[3\mu(h_2^2 - h_1^2)w_{0z} + \gamma(h_1 + h_2) + \frac{\rho}{4}(h_2^4 - h_1^4)B^2\right]_z, \tag{32}$$

$$(h_1^2)_t + (h_1^2w_0)_z = \frac{h_1h_2(2p_oh_1h_2 - 2\gamma(h_1 + h_2) + \rho h_1h_2B^2(h_2^2 - h_1^2))}{2\mu(h_2^2 - h_1^2)}, \tag{33}$$

$$(h_2^2)_t + (h_2^2w_0)_z = \frac{h_1h_2(2p_oh_1h_2 - 2\gamma(h_1 + h_2) + \rho h_1h_2B^2(h_2^2 - h_1^2))}{2\mu(h_2^2 - h_1^2)}, \tag{34}$$

$$\rho[h_2^2(h_2^2B)_t - h_1^2(h_1^2B)_t] + \rho w_0[h_2^2(h_2^2B)_z - h_1^2(h_1^2B)_z] + \frac{\rho}{\mu}p_oBh_1^2h_2^2$$
$$-\frac{\rho\gamma Bh_1h_2}{\mu}(h_1 + h_2) + \frac{\rho^2B^3h_1^2h_2^2}{2\mu}(h_2^2 - h_1^2) = \left(\mu(h_2^4 - h_1^4)B_z\right)_z. \tag{35}$$

The boundary conditions are

$$h_1(0) = h_{10}, \quad h_2(0) = h_{20}, \quad w_0(0) = W_f, \quad w_0(L) = W_d, \quad B(0) = B_0, \quad B(L) = B_L, \tag{36}$$

where the subscripts f and d denote feed and draw conditions, respectively; for the unsteady problem suitable initial conditions must also be prescribed.

It is worth pointing out that these are the lowest-order boundary conditions appropriate to our leading-order model, and that the full Navier–Stokes problem described by (1)–(4) would require additional boundary data to be properly posed.

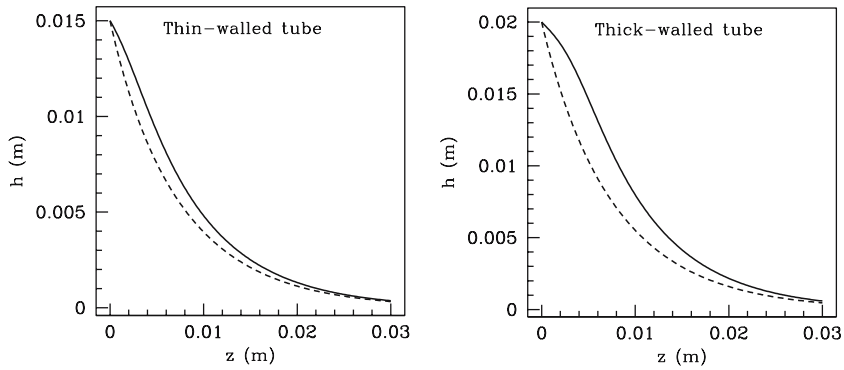

Fig. 4 Numerical calculations of the effects of fibre rotation on outer capillary radius. (Draw length $L = 0.03\,\text{m}$, temperature $T = 2{,}200°\text{C}$, dynamic viscosity $\mu = 4{,}340\,\text{Pa s}$, density $\rho = 2{,}200\,\text{kg/m}^3$, draw speed $W_d = 25\,\text{m/min}$, feed speed $W_f = 15\,\text{mm/min}$, rotation rate $\Omega = 334\,\text{rpm}$.) Each diagram shows the quantity h_2 for fibre pulls with and without rotation. left diagram: thin-walled tube ($h_1(0) = 0.01\,\text{m}$, $h_2(0) = 0.015\,\text{m}$), right diagram: thick-walled tube ($h_1(0) = 0.01\,\text{m}$, $h_2(0) = 0.02\,\text{m}$). In both cases, the lower (broken) of the two curves is the case with no rotation. The upper (solid) curves both show a 'bulge' resulting from the effect of fibre rotation

3 Numerical analysis

Presently we will analyse the Eqs. 32–36 in detail. We first confirm that the act of imparting a rotation to a capillary has noticeable consequences for its geometry. As noted above, rotation is essential to reduce PMD (as achieved experimentally in [8]). If the fibre geometry alters as a result of this rotation, the possibility arises of using fibre rotation as an additional control parameter in the drawing process.

To confirm that non-negligible geometry changes do indeed occur, the full leading-order (dimensional) steady-state equations (28)–(31) were solved using standard library routines. The usual convergence and accuracy tests were carried out to ensure that the numerical results were trustworthy.

To give a general indication of the sort of effect that rotation may have, Fig. 4 shows numerical calculations whose results demonstrate the effects of fibre rotation on both a thin- and a thick-walled capillary with typical drawing parameters. The feed and draw speeds were taken to be $W_f = 15\,\text{mm/min}$ and $W_d = 25\,\text{m/min}$, the draw length was $L = 0.03\,\text{m}$, the rotation imparted was $\Omega/\epsilon = 334\,\text{rpm}$ and an internal capillary radius of $h_{10} = 0.01\,\text{m}$ and external radii of $h_{20} = 0.015\,\text{m}$ (thin-walled tube) and $h_{20} = 0.02\,\text{m}$ (thick-walled tube) were used. We assumed that the glass involved was silica Suprasil F300, a high-quality glass commonly used in the production of commercial low-loss optical fibres. The physical properties used for the computations were taken from [12]. F300 has a density of $2200\,\text{kg/m}^3$. We assumed a draw temperature of 2,200°C, a surface tension of 0.3 N/m and (since the viscosity of F300 is generally unavailable) a viscosity law (the "Fulcher law") of the form

$$\mu = 0.1 \times 10^{-6.24+26900/(T+273)}\ \text{Pa s}, \tag{37}$$

where the temperature T is measured in Celsius, so that in this case $\mu \sim 4{,}340\,\text{Pa s}$. Unless otherwise stated, we shall henceforth assume that the furnace temperature is constant along its length, thus removing the z-dependence from the viscosity, which is now directly related to the furnace temperature. The assumption that the furnace temperature is constant simplifies the analysis, although if the temperature were non-constant (but known) the effects of variable temperature could easily be included. Furnace manufacturers routinely claim that their furnaces operate at constant temperature, but checking this is extremely difficult as no thermocouple can survive even normal furnace temperatures. For more discussion concerning the variations in the furnace temperature and some experimental measurements, see [17]. It should also be pointed out that the viscosity model (37) is not known to be correct, and since the viscosity depends exponentially on the temperature of the fluid, large errors are possible. Needless to say, both the model and the method are applicable to general fluids.

The results in Fig. 4, where the broken and solid lines represent, respectively, the outer radius profile without and with rotation, demonstrate that rotation causes the outer fibre radius to increase, predominantly at the top of the furnace.

It may be confirmed numerically that the general effect of rotating the preform as it enters the furnace is to increase both the inner and outer radii of the fibre along the entirety of the draw length, implying that the final fibre dimensions are larger than if the fibre were not rotated. In the case of the thin-walled tube the dimensions at $z = L$ of the outer diameter were increased by 20%, and for the thick-walled tube they were increased by 11%.

Fibre rotation may thus potentially be used as an additional control in the drawing process, since it is the fibre dimensions at the end of the furnace that primarily concern us. We also note that rotation appears to act on the fibre in a way that counteracts the effects of surface tension, a force that tends to close the air holes in the fibre. As well as reducing birefringence, rotation may thus, for example, allow fibres to be drawn at increased temperatures. This is advantageous from a manufacturing point of view as fibres drawn at high temperatures are often less vulnerable to breakage during drawing.

It is also clear from Fig. 4 that a thick-walled tube experiences a greater deformation than a thin-; this is largely because the initial outer radius of the thick-walled capillary is larger than that of the thin-walled capillary, and partly because of mass-conservation conditions imposed. To gain more insight into the results, we have compared the magnitudes of respective changes in fibre radii as a result of spinning different fibre types. This reveals that, for both thin- and thick–walled tubes, the inner radius increases more than the outer. The fluid near to the outer edges of the fibre rotates at the same angular frequency (and thus with a faster linear speed) and therefore experiences more of an effect due to the rotation than the fluid near to the central hole. The displacement of the outer edge of the fibre, coupled with mass-conservation requirements, requires that the inner portions of the fibre must undergo larger changes in radial position.

From the above numerical analysis, it is already clear that we are justified in investigating the effects of the fibre rotation on the fibre geometry more closely. This analysis will now be carried out.

4 Asymptotic limits of the model

4.1 General comments

As we have seen, the key non-dimensional parameters in the model are

$$\epsilon = \frac{h}{L}, \quad \mathrm{Re} = \frac{LW\rho}{\mu_0}, \quad \mathrm{Fr} = \frac{W^2}{gL}, \quad S = \frac{\Omega L}{W}.$$

Below we speak of Re being $\ll 1$. Whilst this can be theoretically achieved in a variety of ways (i.e., $\rho \ll 1$), it is realised in practice by pulling at low temperatures (and hence at relatively large viscosities). Conversely, $\mathrm{Re} = O(1)$ implies a small viscosity and thus a high draw temperature. For standard furnaces, the draw temperature is typically $T = 2{,}000°\mathrm{C}$ and thus, for standard draw speeds and furnace lengths, Re is invariably $\ll 1$.

The preform rotation rate is measured by S. With (say) $L \sim 0.03\,\mathrm{m}$ and $W \sim 3\,\mathrm{m/s}$, $S = O(1)$ corresponds to rotating the fibre at approximately 1,000 rpm, a rate that can be achieved in practice. This however, is near to the current practical upper limit. For a typical research-grade drawing tower, if the rotation rate is increased beyond about 2,000 rpm, the alignment of the preform in the furnace becomes critical, and perturbations in this alignment rapidly develop into undesirable radial oscillations [6].

When the effects of gravity are ignored, $\frac{1}{\mathrm{Fr}}$ is zero. When we wish to neglect inertial effects the term $w_0 w_{0z}$ is set equal to zero.

Our main concern will be steady-state solutions of the model. A transient analysis may be carried out, but we postpone details of this to a further study.

First, we note that the rotation equation (31) decouples from the momentum equation (28) when $S \ll 1$. To estimate the amount of rotation that has to be imparted for the geometry to be affected, we consider the steady-state

case for solid fibres, when the inertial force term, along with surface tension, gravity and hole overpressure, are neglected. The z-momentum equation (28) becomes

$$3\bar{\mu}(\bar{h}_2^2\bar{w}_{0\bar{z}})_{\bar{z}} = -\frac{1}{4}\mathrm{Re}S^2(\bar{h}_2^4\bar{B}^2)_{\bar{z}},$$

since the non-dimensional variables in this equation have already been suitably scaled, they may be set to unity to reveal that rotation affects the fibre geometry when

$$S \sim \sqrt{\frac{12\bar{\mu}}{\mathrm{Re}}},$$

or, in physical variables,

$$\frac{\Omega}{\epsilon} \sim \frac{2}{h}\sqrt{\frac{3\bar{\mu}\mu_0 W}{L\rho}}.$$

This expression confirms one's intuition that fibres with a large viscosity require rapid rotation to induce a geometry change.

Using typical parameter values, we find from numerical experiments that rotation starts to affect the final fibre dimensions when $\Omega/\epsilon \approx 3{,}000\,\mathrm{rpm}$. Though spinning is not normally used during holey-fibre manufacture, solid fibres are routinely rotated. We conclude that, though rotating a solid preform at rates currently used in fibre manufacture will not significantly affect the fibre geometry [18], the hollow geometry of holey fibres or capillary tubes may be seriously affected at rotation rates required to significantly reduce PMD.

4.2 The twist periodicity

It is useful to be able to estimate how rapidly a preform must be rotated to reduce PMD. The length scale of the pitch required in the final fibre will depend on the wavelength window of the light travelling in the fibre and the consequent beat length of the interference.

In the physically realistic case where $S \sim O(1)$ and $\mathrm{Re} \ll 1$ we may determine the distance between successive 2π rotations in the fibre, (the "twist periodicity") by defining the angle θ to be the number of radians through which a fluid particle rotates as it traverses the z-axis. If we know the rate at which θ changes with time at the end of the draw length, then from this we can directly calculate the final twist periodicity d using

$$d(z) = \frac{2\pi\, w_0(z)}{\partial\theta/\partial t'}, \tag{38}$$

where t' denotes the time that a given point in the fibre has been present in the furnace.

To derive an equation for θ we follow a fluid element along the evolving preform. Thus

$$\theta_{t'} + w_0(z)\theta_z = B(z), \tag{39}$$

with

$$\theta(0, t') = B(0)t'.$$

Thus

$$\theta(z, t') = B(0)t' + \int_0^z \frac{[B(z') - B(0)]}{w_0(z')}\,\mathrm{d}z'.$$

Substituting this in (38) and evaluating at the point $z = L$ now gives the final twist periodicity

$$d(L) = \frac{2\pi\, W_d}{\frac{\partial\theta}{\partial t'}\,|_{z=L}} = \frac{2\pi\, W_d}{B(0)}. \tag{40}$$

We note that the twist periodicity is independent of the functional form of the fibre radius, fluid velocity and angular frequency. The details of the drawing process manifest themselves only through the draw speed, W_d and

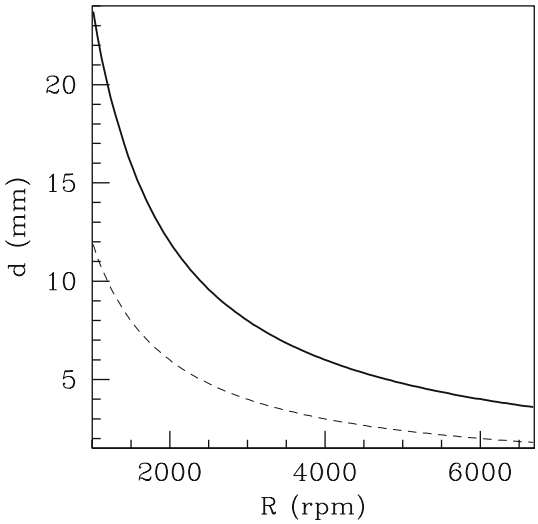

Fig. 5 Variation in twist periodicity in a solid fibre with rotation rate shown for two realistic draw speeds. The upper curve corresponds to a draw speed of 48 m/min ($\beta = 8.07$), and the lower to a draw speed of 24 m/min ($\beta = 7.38$). In both cases the feed speed is 15 mm/min

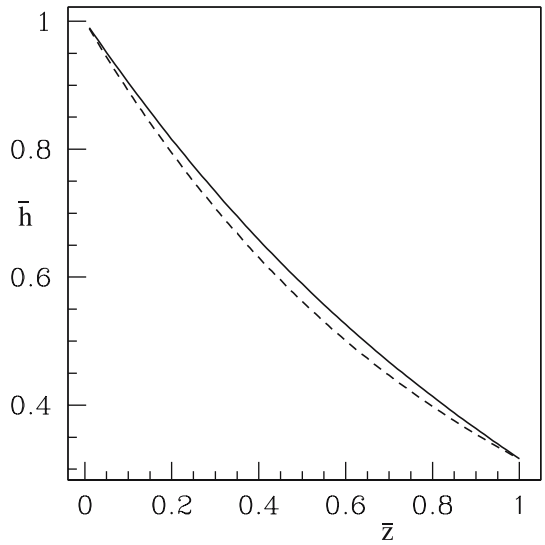

Fig. 6 The effect of a small surface tension on the radius of a solid fibre. The lower (broken) of the two curves shows the fibre radius without surface tension, and the upper (solid) curve represents the fibre radius with a small surface tension added. Both $\bar{h}$ and $\bar{z}$ are non-dimensional quantities

the initial rotation rate, $B(0)$. This is consistent with the fact that, with $\bar{B}(1) = 0$, the twist periodicity should be wholly determined by the draw speed and the rotation rate at $z = 0$. Assuming a steady state means that the same number of 2π-rotations that pass any ordinate $\bar{z}$ per unit of time must be constant and equal to the rotation rate at the feed. The twist periodicity should therefore be determined simply by how rapidly the fibre is being "stretched out". At $\bar{z} = 1$ this speed is the draw speed, thus explaining the form of the expression (40). Naturally, if either d or w were time-dependent this conclusion would be false. Figure 5 shows how d varies with applied rotation rate and with draw speed. Since a typical fibre beat length in a non-linear holey fibre is approximately a few mm, we conclude that rotation rates of at least 4,000 rpm would be required to significantly reduce PMD.

The expression (40) is valid for both solid fibres and capillaries. For holey fibres matters are complicated by the fact that, in general, $\bar{v}_0 \neq \bar{B}(\bar{z}, \bar{t})\bar{r}$. One might hypothesise, however, that this relationship will be at least approximately correct. Indeed, it was found during experiments recently performed at the Optoelectronics Research Centre, University of Southampton where, for the first time, holey fibres were rotated, that not only was PMD reduced, but the measured twist periodicity was in virtually exact agreement with (40) (see [8]).

4.3 Rotation of a solid fibre

We now analyse the steady-state solid-fibre limit, where we set $\bar{h}_1 = 0$, $\bar{h}_2 = \bar{h}$ and $\bar{w}_0 = \bar{w}$. We ignore the effects of inertia, gravity, hole overpressure and surface tension so that we may gain an insight into the physics of the problem from relatively simple equations. Equations 28, 30 and 31 give

$$3\bar{\mu}(\bar{h}^2\bar{w}_{\bar{z}})_{\bar{z}} + \frac{\mathrm{Re}S^2}{4}(\bar{h}^4\bar{B}^2)_{\bar{z}} = 0, \quad (\bar{h}^2\bar{w})_{\bar{z}} = 0, \quad \mathrm{Re}\bar{w}\bar{h}^2(\bar{h}^2\bar{B})_{\bar{z}} = \bar{\mu}(\bar{h}^4\bar{B}_{\bar{z}})_{\bar{z}}$$

with $\bar{h}(0) = \bar{h}_0$, $\bar{w}(0) = \bar{W}_f$, $\bar{w}(1) = \bar{W}_d$, $\bar{B}(0) = \bar{B}_0$ and $\bar{B}(1) = \bar{B}_L$.

The limit $\mathrm{Re} = O(1)$, $S^2 \ll 1$ corresponds to a regime where both fibre rotation and glass viscosity are relatively small. In this case the equations may be solved in closed form to yield

$$\bar{h} = \bar{h}_0 \mathrm{e}^{-\frac{\beta\bar{z}}{2}}, \quad \bar{w} = \bar{W}_f \mathrm{e}^{\beta\bar{z}}, \tag{41}$$

and

$$\bar{B} = C \exp\left(\frac{\mathrm{Re}\bar{W}_f \mathrm{e}^{\beta\bar{z}}}{\bar{\mu}\beta}\right) + D(\mathrm{Re}\bar{W}_f \mathrm{e}^{\beta\bar{z}} + \bar{\mu}\beta). \tag{42}$$

Here $\beta = \log(\frac{W_d}{W_f})$, C and D are defined by

$$C = \frac{\mathrm{Re}(\bar{W}_f \bar{B}_L - \bar{W}_d \bar{B}_0) + \bar{\mu}\beta(\bar{B}_L - \bar{B}_0)}{\mathrm{Re}\left(\bar{W}_f \bar{H}_d - \bar{W}_d \bar{H}_f\right) + \bar{\mu}\beta(\bar{H}_d - \bar{H}_f)},$$

$$D = \frac{\bar{B}_0 \bar{H}_d - \bar{B}_L \bar{H}_f}{\mathrm{Re}\left(\bar{W}_f \bar{H}_d - \bar{W}_d \bar{H}_f\right) + \bar{\mu}\beta(\bar{H}_d - \bar{H}_f)},$$

and $\bar{H}_f = \exp\left(\frac{\mathrm{Re}\bar{W}_f}{\bar{\mu}\beta}\right)$, $\bar{H}_d = \exp\left(\frac{\mathrm{Re}\bar{W}_d}{\bar{\mu}\beta}\right)$.

A closed-form solution is also available when both the fibre rotation and the glass viscosity are relatively large so that $S^2 = O(1)$ and $\mathrm{Re} \ll 1$. We find that $\bar{h}$ and $\bar{w}$ are still given by (41), but

$$\bar{B} = \frac{1}{\mathrm{e}^{2\beta} - 1}((\bar{B}_L - \bar{B}_0)\mathrm{e}^{2\beta\bar{z}} - \bar{B}_L + \bar{B}_0 \mathrm{e}^{2\beta}). \tag{43}$$

Some interesting physical conclusions follow from these two cases. It may easily be shown that (42) predicts that the rotation rate is not monotonic and $\bar{B}$ attains a maximum at

$$\bar{z} = \frac{1}{\beta} \log\left[\frac{\bar{\mu}\beta}{\bar{W}_f \mathrm{Re}} \log\left(\frac{-D\beta\bar{\mu}}{C}\right)\right].$$

For example, with $\bar{\mu} = 1$, $\mathrm{Re} = 1$, $\bar{W}_f = 1/100$, $\bar{W}_d = 1$, $\bar{B}_0 = 1$ and $\bar{B}_L = 0$ the maximum in the rotation rate occurs at $\bar{z} \simeq 0.489$.

In contrast, the rotation rate given by (43) (where the effects of fibre rotation dominate those due to viscosity) is evidently monotonic. For most practical fibre-draws the ratio β is large. Under these circumstances (43) shows that $\bar{B} \sim \bar{B}_0$ for most of the draw, changing to assume the value $\bar{B}_L$ at $\bar{z} = 1$ only in a boundary layer near to the end of the draw.

4.3.1 A solid fibre with small surface tension

For solid fibres with $\bar{\gamma} \ll 1$ we may carry out a regular perturbation in $\bar{\gamma}$. With the effects of inertia, gravity and hole overpressure ignored, we find that

$$3\bar{\mu}(\bar{h}^2 \bar{w}_{\bar{z}})_{\bar{z}} + \bar{\gamma}\bar{h}_{\bar{z}} + \frac{\mathrm{Re}S^2}{4}(\bar{h}^4 \bar{B}^2)_{\bar{z}} = 0, \tag{44}$$

$$(\bar{h}^2 \bar{w})_{\bar{z}} = 0, \tag{45}$$

$$\mathrm{Re}\bar{w}\bar{h}^2(\bar{h}^2 \bar{B})_{\bar{z}} = \bar{\mu}(\bar{h}^4 \bar{B}_{\bar{z}})_{\bar{z}}. \tag{46}$$

Setting

$$\bar{h} = \bar{h}_0 + \bar{\gamma}\bar{h}_{01} + \cdots, \quad \bar{w} = \bar{w}_0 + \bar{\gamma}\bar{w}_{01} + \cdots, \quad \bar{B} = \bar{B}_0 + \bar{\gamma}\bar{B}_{01} + \cdots,$$

setting $S = 1$ (and assuming that Re $\ll 1$, i.e., relatively large viscosity) we find that $\bar{h}_0$, $\bar{w}_0$ and $\bar{B}_0$ are given by (41) and (42), respectively, and

$$\bar{h}_{01} = \frac{\mathrm{e}^{-\frac{\beta\bar{z}}{2}}\left(3F\bar{\mu}\beta\bar{W}_f - \mathrm{e}^{-\frac{\beta\bar{z}}{2}} + 3G\bar{\mu}\beta\bar{W}_f\bar{z}\right)}{3\bar{\mu}\beta\bar{W}_f}, \tag{47}$$

$$\bar{w}_{01} = \frac{\mathrm{e}^{\frac{\beta\bar{z}}{2}}\left(3J\bar{\mu}\beta\bar{h}_0\mathrm{e}^{\frac{\beta\bar{z}}{2}} - 6G\bar{\mu}\beta\bar{W}_f\bar{z}\mathrm{e}^{\frac{\beta\bar{z}}{2}} + 2\right)}{3\bar{\mu}\beta\bar{h}_0} \tag{48}$$

and

$$\begin{aligned}\bar{B}_{01} = [&36G\bar{B}_L\bar{\mu}\bar{W}_f\mathrm{e}^{2\beta\bar{z}} - 72G\bar{B}_L\bar{\mu}\beta\bar{W}_f\bar{z}\mathrm{e}^{2\beta\bar{z}} + 32\bar{B}_L\mathrm{e}^{\frac{3\beta\bar{z}}{2}} + 72G\bar{B}_0\bar{\mu}\beta\bar{W}_f\bar{z}\mathrm{e}^{2\beta\bar{z}}\\ &-36G\bar{B}_0\bar{\mu}\bar{W}_f\mathrm{e}^{2\beta\bar{z}} - 32\bar{B}_0\mathrm{e}^{\frac{3\beta\bar{z}}{2}} + 9K\bar{\mu}\bar{W}_f\bar{h}_0\mathrm{e}^{2\beta(1+\bar{z})} - 9K\bar{\mu}\bar{W}_f\bar{h}_0\mathrm{e}^{2\beta\bar{z}}\\ &+18M\bar{\mu}\beta\bar{W}_f\bar{h}_0\mathrm{e}^{2\beta} - 18M\bar{\mu}\beta\bar{W}_f\bar{h}_0]/(18\bar{\mu}\beta\bar{W}_f\bar{h}_0(\mathrm{e}^{2\beta} - 1))\end{aligned}$$

where F, G, J, K and M are constants defined by

$$F = \frac{1}{3\bar{\mu}\beta\bar{W}_f}, \quad G = \frac{1 - \mathrm{e}^{\frac{\beta}{2}}}{3\bar{\mu}\beta\bar{W}_f\mathrm{e}^{\frac{\beta}{2}}}, \quad J = -\frac{2}{3\bar{\mu}\beta\bar{h}_0},$$

$$\begin{aligned}K = &4\left((\bar{B}_L - \bar{B}_0)(3 - 6\beta)\mathrm{e}^{2\beta} + 8(\bar{B}_0 - \bar{B}_L)(\mathrm{e}^{\frac{3\beta}{2}} + \mathrm{e}^{\beta} + \mathrm{e}^{\frac{\beta}{2}}) + 3(\bar{B}_0 - \bar{B}_L)\right)/9\bar{\mu}\beta\bar{W}_f\bar{h}_0\mathrm{e}^{\frac{\beta}{2}}\\ &\left(\mathrm{e}^{\frac{7\beta}{2}} + \mathrm{e}^{3\beta} + \mathrm{e}^{\frac{5\beta}{2}} + \mathrm{e}^{2\beta} - \mathrm{e}^{\frac{3\beta}{2}} - \mathrm{e}^{\beta} - \mathrm{e}^{\frac{\beta}{2}} - 1\right)\end{aligned}$$

and

$$M = \frac{4(\bar{B}_0 - \bar{B}_L)\mathrm{e}^{\frac{3\beta}{2}}}{9\bar{\mu}\beta\bar{W}_f\bar{h}_0\left(\mathrm{e}^{\frac{7\beta}{2}} + \mathrm{e}^{3\beta} + \mathrm{e}^{\frac{5\beta}{2}} + \mathrm{e}^{2\beta} - \mathrm{e}^{\frac{3\beta}{2}} - \mathrm{e}^{\beta} - \mathrm{e}^{\frac{\beta}{2}} - 1\right)}.$$

These results demonstrate that the presence of surface tension acts to push the fibre out along the majority of the draw length ($\bar{h}_{01}$ is always positive) except at the very ends of the draw length, where is it required to retain a given radius through the mass-conservation condition (see Fig. 6). At first such expansion seems counter-intuitive, but can be understood by considering the velocity boundary conditions.

For capillaries, numerical results confirm that, as one might expect (and is observed experimentally), surface tension always acts against the rotation and tends to reduce the surface area of the fibre; i.e., $\bar{h}_1$ and $\bar{h}_2$ are always decreased.

4.3.2 Rotation boundary layer

If the fibre draw speed is increased, while the feed speed remains fixed, the fibre thins rapidly. Since the results for h and w typically depend exponentially upon the distance along the furnace, the fibre thins increasingly rapidly as it passes down the furnace. As β, the ratio of the draw speed to the feed speed increases, the radius decreases rapidly, causing the rotation to be preserved further along the draw length (by conservation of angular momentum). This rotation is then lost rapidly towards the end of the draw length at $z = L$. For draw speeds that are large compared to the feed speed, we therefore expect a boundary layer in $\bar{B}$ near to $z = L$.

Numerical simulations of the final dimensional equations confirm that, under these circumstances, a boundary layer exists in the solution of the angular frequency, $\bar{B}$. To analyse this boundary layer we recall that in nearly all practical cases Re $\ll 1$. For Re $= 0$, $\bar{\gamma} = 0$ and $S = O(1)$, the solid-fibre equations become

$$3\bar{\mu}(\bar{h}^2\bar{w}_{\bar{z}})_{\bar{z}} = 0, \quad (\bar{h}^2\bar{w})_{\bar{z}} = 0, \tag{49}$$

and

$$\bar{\mu}(\bar{h}^4\bar{B}_{\bar{z}})_{\bar{z}} = 0. \tag{50}$$

Thus (with $\bar{\mu} = 1$) we have $\bar{h} = \bar{h}_0 \mathrm{e}^{-\frac{\beta\bar{z}}{2}}$ and $\bar{w} = \bar{W}_f \mathrm{e}^{\beta\bar{z}}$ so that (50) gives

$$2\bar{B}_{\bar{z}} - \phi \bar{B}_{\bar{z}\bar{z}\bar{z}} = 0,$$

with $\phi = 1/\beta$. Bearing in mind that typically $W_d/W_f \sim 10^5$ so that $\beta \sim 12$, the origin of the rotation boundary layer is clear. We find that

$$\bar{B} = \frac{\bar{B}_0(\mathrm{e}^{2\beta} - \mathrm{e}^{2\beta\bar{z}})}{\mathrm{e}^{2\beta} - 1}$$

so that the thickness of the rotation boundary layer is $O(1/\beta)$. Standard boundary-layer analyses may also be undertaken for more general forms of the governing equations than (49) and (50). These invariably suggest that, for realistic fibre drawing conditions, the rotation boundary layer is ubiquitous.

4.4 Rotation of capillary tubes

Having analysed solid fibres under rotation, we now consider the effects that rotation might have on drawn capillary tubes. Under normal circumstances, surface tension promotes hole closure, so that holes required in the final structure may cease to exist. On the other hand, there are circumstances when it is desired to draw a capillary containing an extremely small hole. Our principal concern will therefore be to analyse the fate of a small hole in a capillary and to consider the relative merits of fibre rotation and internal pressurisation as mechanisms for preventing hole closure.

4.4.1 Closing of a small hole in a capillary

Small holes are particularly prone to closure under the effects of surface tension. Since the survival of discrete holes in a capillary or a holey fibre is often a key matter of interest, we therefore now study a case where $\bar{h}_1 = O(\delta)$ where $\delta \ll 1$ is a positive small parameter, taking $\mathrm{Re} = O(\delta^2)$, $S = O(1)$, $\bar{\gamma} = O(1)$, $\bar{\mu} = O(1)$, $\bar{h}_2 = O(1)$ and $\bar{w}_0 = O(1/\delta)$ (large draw ratio). The steady leading-order equations in the absence of inertia and gravity give

$$\bar{h}_2 = \bar{h}_{20}\mathrm{e}^{-\beta\bar{z}/2}, \quad \bar{w}_0 = \bar{W}_f \mathrm{e}^{\beta\bar{z}} \tag{51}$$

and

$$2\bar{w}_0\bar{h}_{1\bar{z}} + \bar{h}_1\bar{w}_{\bar{z}} = -\frac{\bar{\gamma}}{\bar{\mu}},$$

so that

$$\bar{h}_1 = \frac{1}{\bar{\mu}\beta\bar{W}_f}[\bar{\gamma}\mathrm{e}^{-\beta\bar{z}} + (\bar{\mu}\beta\bar{h}_{10}\bar{W}_f - \bar{\gamma})\mathrm{e}^{-\beta\bar{z}/2}].$$

The hole size thus decreases monotonically (provided $\bar{h}_1$ remains positive), with

$$\bar{h}_1(1) = \frac{\mathrm{e}^{-\beta/2}}{\bar{\mu}\beta\bar{W}_f}[\bar{\gamma}(\mathrm{e}^{-\beta/2} - 1) + \bar{\mu}\beta\bar{W}_f\bar{h}_{10}],$$

so that the hole survives whenever

$$\bar{h}_{10} > \frac{\bar{\gamma}}{\bar{\mu}\beta\bar{W}_f}(1 - \mathrm{e}^{-\beta/2}).$$

Suppose we now attempt to retain the hole structure by pressurizing the hole. Examining the equations reveals that a pressure of $O(1/\delta)$ is required to affect the equation for $\bar{h}_1$, which then becomes

$$2\bar{w}_0\bar{h}_{1\bar{z}} + \bar{h}_1\bar{w}_{\bar{z}} = -\frac{\bar{\gamma}}{\bar{\mu}} + \frac{\bar{p}_o\bar{h}_1}{\bar{\mu}}. \tag{52}$$

Since $\bar{h}_2$ and $\bar{w}_0$ are still given by (51), (52) may be solved to yield

$$\bar{h}_1 = \exp\left(-\frac{\beta\bar{z}}{2} - \frac{k}{2}\mathrm{e}^{-\beta\bar{z}}\right)\left[\bar{h}_{10}\mathrm{e}^{k/2} - \frac{\bar{\gamma}}{2\bar{\mu}\bar{W}_f}\int_0^{\bar{z}} \exp\left(-\frac{\beta\xi}{2} + \frac{k}{2}\mathrm{e}^{-\beta\xi}\right)\,\mathrm{d}\xi\right]$$

where $k = \bar{p}_o/(\bar{\mu}\beta\bar{W}_f)$. Now consider the specific case where $\bar{W}_f = w_f$, $\bar{W}_d = w_d/\delta$, $\bar{h}_{10} = H_{10}\delta$, $\bar{p}_o = P/\delta$, and $V = w_d/w_f$. Then $\beta = \log(V/\delta)$ and $k = P/(\bar{\mu}w_f\delta\log(V/\delta))$. We now find that

$$I(\bar{z}) = \int_0^{\bar{z}} \exp\left(-\frac{\beta\xi}{2} + \frac{k}{2}\mathrm{e}^{-\beta\xi}\right)\,\mathrm{d}\xi = \frac{1}{\beta}\int_{\mathrm{e}^{-\beta\bar{z}}}^1 \zeta^{-1/2}\mathrm{e}^{k\zeta/2}\,\mathrm{d}\zeta,$$

and thus

$$I(\bar{z}) = \frac{\sqrt{2\pi}}{\beta\sqrt{-k}}\left[\mathrm{erf}\left(\sqrt{-\frac{k}{2}}\right) - \mathrm{erf}\left(\sqrt{-\frac{k\mathrm{e}^{-\beta\bar{z}}}{2}}\right)\right].$$

For $x \gg 1$ we have

$$\mathrm{erf}(x) \sim 1 + \frac{\mathrm{e}^{-x^2}}{\sqrt{\pi}}\left(-\frac{1}{x} + \frac{1}{2x^3} - \frac{3}{4x^5} + O(x^{-7})\right)$$

and we also note that $k \gg 1$ and $k\mathrm{e}^{-\beta\bar{z}} \gg 1$ for all $\bar{z} \in [0, 1]$ *except* exponentially close to $\bar{z} = 1$. Thus so long as $\bar{z}$ is not near to 1, we have

$$I(\bar{z}) \sim \frac{2}{\beta k}\left[\mathrm{e}^{k/2} - \exp\left(\beta\bar{z}/2 + \frac{k}{2}\mathrm{e}^{-\beta\bar{z}}\right)\right] + \frac{2}{\beta k^2}\left[\mathrm{e}^{k/2} - \exp\left(3\beta\bar{z}/2 + \frac{k}{2}\mathrm{e}^{-\beta\bar{z}}\right)\right] + \cdots,$$

the one-term approximation yielding good agreement with the exact value for most large values of β. Using this, we find that $\bar{h}_1$ may be approximated by

$$\bar{h}_1 \sim \mathrm{e}^{-\frac{\beta\bar{z}}{2} + \frac{k}{2}(1-\mathrm{e}^{-\beta\bar{z}})}\left[\delta\bar{H}_{10} - \frac{\bar{\gamma}}{\bar{\mu}w_f\beta k}\left(1 - \mathrm{e}^{\beta\bar{z}/2 + \frac{k}{2}(\mathrm{e}^{-\beta\bar{z}}-1)}\right)\right].$$

Let us examine how $\bar{h}_1$ depends on the pressurization somewhere away from the two ends of the draw. Since $\beta = \log(V/\delta) \gg 1$ and $k = O((\delta\log\delta)^{-1})$, when $\bar{z}$ is close neither to 0 nor 1 we have

$$\bar{h}_1 \sim \mathrm{e}^{k/2}\left[\delta\bar{H}_{10} - \frac{\bar{\gamma}}{\bar{\mu}w_f\beta k}\right].$$

Since $k \gg 1$, we see that $\bar{h}_1$ is "exponentially sensitive" to the amount of pressurisation used, so that unless the pressure in the hole can be controlled with unerring accuracy, the capillary will "explode" or the hole will close.

Our observations of the dependence of hole diameter on internal hole pressure suggest that pressure may not be a robust control mechanism to prevent hole closure, but what of rotation? When overpressure is absent but the capillary is rotated, we study the small-hole/large-draw ratio case where $\bar{h}_1 = O(\delta)$ (where $\delta \ll 1$), $\mathrm{Re} = O(\delta^2)$, $S = O(1)$, $\bar{\gamma} = O(1)$, $\bar{\mu} = O(1)$, $\bar{h}_2 = O(1)$ and $\bar{w}_0 = O(1/\delta)$. The rotation appears to leading order in the equation for $\bar{h}_1$ when $\bar{B} = O(\delta^{-3/2})$, in which case the governing equations, for constant $\bar{\mu}$, are

$$\left[3\bar{\mu}\bar{h}_2^2\bar{w}_{0\bar{z}} + \frac{1}{4}\mathrm{Re}S^2\bar{h}_2^4\bar{B}^2\right]_{\bar{z}} = 0, \quad (\bar{h}_2^2\bar{w}_0)_{\bar{z}} = 0, \quad (\bar{h}_2^4\bar{B}_{\bar{z}})_{\bar{z}} = 0, (\bar{h}_1^2\bar{w}_0)_{\bar{z}} = \frac{\bar{h}_1}{2\bar{\mu}}[-2\bar{\gamma} + \mathrm{Re}S^2\bar{B}^2\bar{h}_1\bar{h}_2^2].$$

Further analysis is rendered awkward by the fact that these equations do not possess a closed-form solution, but bearing in mind the ubiquity of the boundary-layer behaviour of $\bar{B}$ established above, we may simplify the problem assuming that the spin is constant and equal, say, to $\bar{B}_0$. We now find that

$$\bar{w}_0 = K(1 + C\mathrm{e}^{A\bar{z}})^{1/2}, \quad \bar{h}_2 = \sqrt{\frac{AK}{2Q^2}}(1 + C\mathrm{e}^{A\bar{z}})^{-1/4},$$

where $Q^2 = \mathrm{Re}S^2\bar{B}_0^2/12\bar{\mu}$, the constants A and K satisfy

$$A = \frac{2Q^2\bar{h}_{20}^2(1+C)}{\bar{W}_f}, \quad K = \bar{W}_f(1+C)^{-1/2}$$

and the constant C is determined by solving

$$\left(\frac{\bar{W}_d}{\bar{W}_f}\right)^2 - 1 = \frac{C}{1+C}\left[\exp\left(\frac{2Q^2\bar{h}_{20}^2(1+C)}{\bar{W}_f}\right) - 1\right],$$

which may easily be shown to have a unique positive solution for C. The governing equation for $\bar{h}_1$ is now

$$2\bar{h}_{1\bar{z}}\bar{w}_0 = \bar{h}_1\bar{w}_{0\bar{z}} - \frac{\bar{\gamma}}{\bar{\mu}} + 6Q^2\bar{h}_2^2\bar{h}_1,$$

and thus

$$\bar{h}_1 = \frac{\mathrm{e}^{3A\bar{z}/2}}{(1+C\mathrm{e}^{A\bar{z}})^{7/4}}\left[\bar{h}_{10}(1+C)^{7/4} - \frac{\bar{\gamma}}{2\bar{\mu}K}\int_0^{\bar{z}} \mathrm{e}^{-3A\xi/2}(1+C\mathrm{e}^{A\xi})^{5/4}\,\mathrm{d}\xi\right].$$

As before, we now set $\bar{W}_d = w_d/\delta$, $\bar{W}_f = w_f$, $\bar{h}_{10} = H_{10}\delta$, $\bar{h}_{20} = h_{20}$, $\mathrm{Re} = R\delta^2$ and $\bar{B} = \bar{B}_0/\delta^{3/2}$. We now find that C satisfies

$$\frac{V^2}{\delta^2} - 1 = \frac{C}{1+C}(\mathrm{e}^{\Lambda(1+C)/6\delta} - 1), \tag{53}$$

where $V = w_d/w_f$ and $\Lambda = RS^2\bar{B}_0^2\bar{h}_{20}^2/\bar{\mu}w_f = O(1)$. For $\delta \ll 1$, Eq. (53) may be solved asymptotically to yield

$$C \sim \frac{V^2}{\delta^2}\mathrm{e}^{-\Lambda/6\delta}, \quad K \sim w_f, \quad A \sim \frac{\Lambda}{6\delta}.$$

For $\Lambda = O(1)$ it is now easy to show that

$$\int_0^{\bar{z}} \mathrm{e}^{-\Lambda\xi/4\delta}\left(1 + \frac{V^2}{\delta^2}\mathrm{e}^{-\Lambda(1-\xi)/6\delta}\right)^{5/4}\,\mathrm{d}\xi \sim \frac{4\delta}{\Lambda}[1 - \mathrm{e}^{-\Lambda\bar{z}/4\delta}]$$

and thus in this limit

$$h_1 \sim \frac{\mathrm{e}^{\Lambda\bar{z}/4\delta}}{\left(1 + \frac{V^2}{\delta^2}\mathrm{e}^{\Lambda(\bar{z}-1)/6\delta}\right)^{7/4}}\left[\delta H_{10}\left(1 + \frac{V^2}{\delta^2}\mathrm{e}^{-\Lambda/6\delta}\right)^{7/4} - \frac{2\bar{\gamma}\delta}{\bar{\mu}w_f\Lambda}(1 - \mathrm{e}^{-\Lambda\bar{z}/4\delta})\right]. \tag{54}$$

The exponential dependence of (54) on the rotation rate suggests that, as concluded above for pressurization, active control of hole size via rotation is likely to be extremely difficult from a practical point of view. Note, however, that the analysis that led to (54) assumed that δ was small enough so that $C \ll 1$. For many practical fibre draws, the small parameter δ may be identified with the quantity $1/\beta$, which, since $\beta = \log(\bar{W}_d/\bar{W}_f)$ is likely to be small though not minute. For example, in many cases, $\delta \sim 0.1$. In these cases, the quantity $C = (V^2/\delta^2)\mathrm{e}^{-\Lambda/6\delta}$ actually turns out to be *large*. What really happens in such cases? Suppose we acknowledge the fact that C is not small by setting $\Gamma = \Lambda/6\delta$ in the exponential and assuming that $\Gamma = O(1)$. We now find that

$$C \sim -\frac{2}{\Gamma}\log\left(\frac{\delta}{V}\right) - 1 - \frac{1}{2\log\delta} + O((\log\delta)^{-2}), \quad A \sim -2\log\left(\frac{\delta}{V}\right) - \frac{\Gamma}{2\log\delta} + O((\log\delta)^{-2}),$$

$$K \sim w_f\sqrt{\frac{\Gamma}{2}}\left(\frac{1}{\sqrt{-\log\delta}} - \frac{\log V}{2(-\log\delta)^{3/2}} + O((-\log\delta)^{-5/2})\right)$$

and thence, to leading order,

$$\bar{h}_1 \sim \frac{\mathrm{e}^{-A\bar{z}/4}}{C^{7/4}}\left[\bar{h}_{10}C^{7/4} - \frac{\bar{\gamma}}{2\bar{\mu}K}\int_0^{\bar{z}} C^{5/4}\mathrm{e}^{-A\xi/4}\,\mathrm{d}\xi\right].$$

From this we conclude that, in this limit

$$\bar{h}_1 \sim \mathrm{e}^{\bar{z}\log\delta/2}\left[H_{10}\delta - \frac{\bar{\gamma}}{w_f\bar{\mu}\log\delta}(\mathrm{e}^{\bar{z}\log\delta/2}-1)\right],$$

an expression that is *independent* of the rotation $\bar{B}_0$, which appears only if one proceeds to the next order. This state of affairs is in marked contrast to the previous exponential dependence and suggests that, in practice, rotation will prove to be a useful control mechanism that may be used to produce capillaries with extremely small holes.

5 Conclusions

The various asymptotic limits considered give good agreement with numerical simulations of the full equations, and make useful predictions regarding the use of fibre rotation to prevent hole collapse under the action of surface tension. They also predict the final twist periodicity of a given drawing scenario. Together these predictions allow an experimenter to predetermine the spin rate according to the required pitch, and hence quantify the effect that the necessary rotation will have on the final fibre geometry. As explained in the introduction, fibre rotation may also be used to reduce PMD and birefringence. Since it transpires that the rotation rates that are required for the latter use are somewhat high for practical purposes (see [10]), most of the specific cases that were studied in detail above discussed the influence of rotation on fibre geometry.

Care must be taken when generalising the physics of the rotation of capillary tubes to the full holey-fibre problem, since the radius of rotation is obviously of critical importance. Although (as explained in the introduction) the relevance of the results to "type one and two" general holey fibres is clear, it must be remembered that not only may general fibres contain extremely complicated geometries, but also that, in general, holes will not be rotated around their centres. Multiple surface interaction effects may also be important as holes merge and/or bifurcate.

The effects of hole overpressure have been investigated and it has been shown that, although this may be a useful control parameter, it is unlikely, by itself, to allow the overall control of hole closure: for further details see [15]. Rotation, however, does provide a useful experimental control so long as the draw ratio is not too large. For more discussion of the rotation of holey fibres see [10], and for general background on the effect of fibre birefringence see [5].

The discussion has assumed that a steady fibre draw is in progress, but fibre draws can sometimes suffer from instabilities. In the worst cases, the fibre may even break during production. A further interesting avenue of exploration would be to determine the effect of fibre rotation on any instability mechanisms that may be present. For further details of the stability of the fibre-drawing process, see [17].

Finally, what overall use is the model that has been developed here and what does the future hold? We regard the model as a first step towards the analysis of the process of drawing rotating holey fibres with arbitrary non-axisymmetric geometry and thereby gaining a theoretical understanding of the reality of drawing microstructured optical fibres. It is interesting to speculate how the modelling process for optical-fibre drawing might evolve over the next few years. Clearly, analysis of the general case, although still a long-term goal, is some distance away. An "extensional-flow" model based on the small aspect ratio of the fibre could be developed as above for the general case, but the advantages of axisymmetry would be lost and the number of free boundaries that would have to be considered would lead to an excessive number of coupled equations. CFD studies have certainly been attempted (see, for example, [19]), but once again, if the number of holes is more than about two or three, the computations involved become extremely complicated. A different modelling philosophy that holds promise is provided by a "two-phase flow" approach where, instead of attempting the daunting task of tracking the evolution of individual holes, the "average behaviour" of the holes in a fibre is predicted (for details, see [17]). Whatever transpires in the coming years, it is clear that the practical importance and use of holey fibres can only increase. Good predictive techniques will therefore continue to be of key importance in the development of the technology.

Acknowledgements T. M. Monro acknowledges the support of a Royal Society University Research Fellowship. The authors would also like to thank C. J. Howls and C. P. Please for useful discussions and insight.

References

1. Ranka JK, Windeler RS, Stentz AJ (2000) Optical properties of high-delta air-silica microstructure optical fibers. Opt Lett 25: 796–798
2. Monro TM, Richardson DJ, Bennett PJ (1999) Developing holey fibers for evanescent field devices. Elect Lett 35: 1188–1189
3. Monro TM, Richardson DJ, Broderick NGR, Bennett PJ (1999) Holey optical fibres: an efficient modal model. IEEE J Lightwave Technol 17: 1093–1102
4. Gordon JI, Kogelnik H (2000) PMD fundamentals: polarization mode dispersion in optical fibres. PNAS 97: 4541–4550
5. Barlow AJ, Ramskov-Hansen JJ, Payne DN (1981) Birefringence and polarization mode-dispersion in spun single-mode fibers. Appl Optics 20: 2962–2967
6. Li MJ, Nolan DA (1998) Fiber spin-profile designs for producing fibers with low polarization mode dispersion. Optics Lett 23: 1659–1661
7. Schuh RE, Shan X, Shamim Siddiqui A (1998) Polarization mode dispersion in spun fibers with different linear birefringence and spinning parameters. IEEE J Lightwave Technol 16: 1583–1588
8. Fuochi M, Hayes JR, Furusawa K, Belardi W, Baggett JC, Monro TM, Richardson DJ (2004) Polarization mode dispersion reduction in spun large mode area silica holey fibres. Opt Express 9:1972–1977. http://www.opticsexpress.org/abstract.cfm?URI=OPEX-12-9-1972
9. Ramos JI (2001) Drawing of annular jets at low Reynolds numbers. Comput Theor Polymer Sci 11: 429–443
10. Voyce CJ, Fitt AD, Monro TM (2004) Mathematical model of the spinning of microstructured fibres. Opt Express 12:5810–5820. http://www.opticsexpress.org/abstract.cfm?URI=OPEX-12-23-5810
11. Howell PD (1997) Extensional thin layer flows. PhD thesis, University of Oxford, Oxford
12. Fitt AD, Furusawa K, Monro TM, Please CP (2001) Modeling the fabrication of hollow fibers: capillary drawing. IEEE J Lightwave Technol 19: 1924–31
13. Doremus RS (1973) Glass science. Wiley, New York
14. Bird RB, Stewart WE, Lightfoot EN (1960) Transport phenomena. Wiley, New York, pp. 83–89
15. Fitt AD, Furusawa K, Monro TM, Please CP, Richardson DJ (2002) The mathematical modelling of capillary drawing for holey fibre manufacture. J Eng Math 43: 201–227
16. Howison S (2005) Practical applied mathematics. Cambridge University Press, Cambridge
17. Voyce CJ (2005) The mathematical modelling of microstructured optical fibres, PhD Thesis. University of Southampton, Southampton
18. Wai PKA, Kath WL, Menyuk CR, Zhang JW (1997) Nonlinear polarization-mode dispersion in optical fibres with randomly varying birefringence. J Opt Am Soc B 14: 2967–2979
19. Xue SC, Large MCJ, Barton GW, Tanner RI, Polodian L, Lwin R (2006) Role of material properties and drawing conditions in the fabrication of microstructured optical fibers. J Lightwave Technol 24: 853–860